Barlowite as a canted antiferromagnet: Theory and experiment

Harald O. Jeschke, Francesc Salvat-Pujol, Elena Gati, Nguyen Hieu Hoang, Bernd Wolf, Michael Lang, John A. Schlueter, and Roser Valentí

Phys. Rev. B **92**, 094417 — Published 10 September 2015

DOI: 10.1103/PhysRevB.92.094417

Barlowite as a canted antiferromagnet: theory and experiment

Harald O. Jeschke,[1] Francesc Salvat-Pujol,[1] Elena Gati,[2] Nguyen Hieu Hoang,[2] Bernd Wolf,[2] Michael Lang,[2] John A. Schlueter,[3] and Roser Valentí[1]

[1] *Institut für Theoretische Physik, Goethe-Universität Frankfurt, Max-von-Laue-Straße 1, 60438 Frankfurt am Main, Germany*
[2] *Physikalisches Institut, Goethe-Universität Frankfurt, Max-von-Laue-Straße 1, 60438 Frankfurt am Main, Germany*
[3] *Division of Materials Research, National Science Foundation, Arlington, Virginia 22230, USA*

We investigate the structural, electronic and magnetic properties of the newly synthesized mineral barlowite $Cu_4(OH)_6FBr$ which contains Cu^{2+} ions in a perfect kagome arrangement. In contrast to the spin-liquid candidate herbertsmithite $ZnCu_3(OH)_6Cl_2$, kagome layers in barlowite are perfectly aligned due to the different bonding environments adopted by F^- and Br^- compared to Cl^-. With the synthesis of this material we unveil a novel design strategy for layered kagome systems with possible exotic magnetic states. Density functional theory calculations and effective model considerations for $Cu_4(OH)_6FBr$ which has a Cu^{2+} site coupling the kagome layers, predict a 3D network of exchange couplings, which together with a substantial Dzyaloshinskii-Moriya coupling lead to canted antiferromagnetic ordering of this compound in excellent agreement with magnetic susceptibility measurements on single crystals yielding $T_N = 15$ K.

PACS numbers: 71.15.Mb, 75.10.Jm, 75.30.Cr, 75.30.Et, 71.20.-b

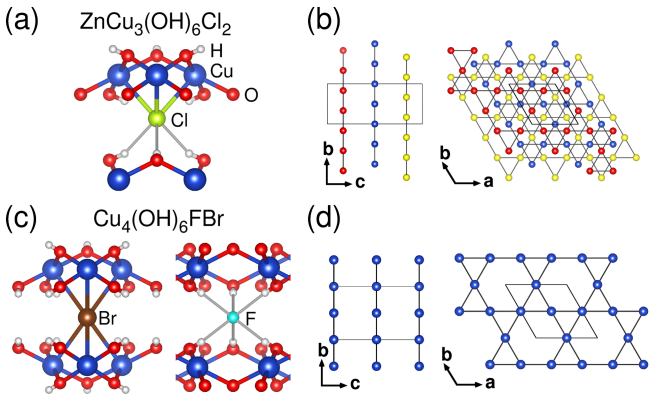

FIG. 1. Chloride environment of herbertsmithite (a) compared to bromide and fluoride environments of barlowite (c). (b) Mix of covalent and hydrogen bonding in $ZnCu_3(OH)_6Cl_2$ leads to three kagome layers shifted with respect to each other, as shown by differently colored Cu^{2+} sites. (d) Preference of Br^- for covalent bonding and of F^- for hydrogen bonding leads to perfect alignment of kagome layers in $Cu_4(OH)_6FBr$ (only Cu(1) sites are shown here).

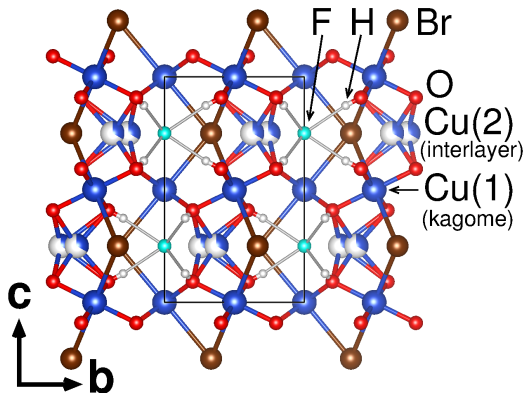

FIG. 2. Crystal structure of $Cu_4(OH)_6FBr$ ($P\,6_3/mmc$ space group, No. 194). Note that the Cu(2) site with Wyckoff position $12j$ is 1/3 filled.

Since the successful synthesis of herbertsmithite ($ZnCu_3(OH)_6Cl_2$)[1], spin-liquid candidates based on spin-1/2 kagome lattices have been intensively investigated in recent years[2,3]. The paratacamite family of compounds has proven to be a fertile ground for kagome materials with different properties. The $Zn_xCu_{4-x}(OD)_6Cl_2$ series of materials has been found to form valence-bond solids due to distortions of the kagome layer in monoclinic space groups[4]. The replacement of Zn^{2+} in $ZnCu_3(OH)_6Cl_2$ by a nonmagnetic ion like Mg^{2+} possibly leads to another spin-liquid candidate[5], as does replacement of $2Cl^-$ by SO_4^{2-}[6]. On the other hand, magnetic ions between the kagome layers lead to compounds that order magnetically[7]. While realizations of quantum spin liquids have been desperately searched for[8], so far, together with the triangular-lattice molecule-based organic materials[9,10], herbertsmithite has been considered one of the best candidates[11]. However, $ZnCu_3(OH)_6Cl_2$ has not been free from controversy as Zn^{2+} and Cu^{2+} are similar in size, and both kagome layers diluted with nonmagnetic Zn^{2+}[3] as well as magnetic Cu^{2+} ions replacing Zn^{2+} between the kagome layers[12] are possible. Therefore, it would be desirable to devise a crystal modification of herbertsmithite that would make the Cu^{2+} and Zn^{2+} sites less similar in order to increase the tendency of Cu^{2+} ions to form the kagome layer as well as the tendency of the nonmagnetic transition metal ion to stay away from the kagome plane. Recently[16] one of the authors introduced the mineral barlowite $Cu_4(OH)_6FBr$ as a layered structure of two-dimensional Cu-based perfect kagome planes and reported the observation of antiferromagnetic order

at low temperatures based on thermodynamic measurements on polycrystalline samples. In the present work we go beyond previous studies and suggest a novel synthetic route to successfully obtain perfect kagome structures, exemplarily realized in the mineral barlowite. Such structures offer an important alternative to herbertsmithite. They are chemically and physically flexible enough so that via doping or application of pressure one can explore not only potential quantum spin liquid behavior at half filling but also other exotic states like flat bands at certain fillings inducing Nagaoka ferromagnetism[13] or the presence of Dirac points at 4/3 filling that could lead to unusual symmetry protected metals or superconductors[14].

Furthermore, we resolve the microscopic origin of the electronic and magnetic behavior of barlowite which has a Cu^{2+} site coupling the kagome layers. Via a combination of density functional theory calculations and magnetic susceptibility measurements we find this material to be a canted antiferromagnet below $T < T_N$ with a canting angle away from the kagome plane of 4.5°.

In herbertsmithite, the Cl^- binding environment is partially covalent, partially hydrogen bonded, as shown in Fig. 1 (a). This leads to a horizontal staggering of kagome layers (Fig. 1 (b)) as Cu^{2+} triangles can be placed either above or below a Cl^- ion, but not both above and below. We suggest using a mixed halide system where the strong hydrogen bond acceptance of the F^- ion is used to create a hydrogen rich pocket with six hydroxyl ions; on the other hand, Br^- can form six covalent bonds to three Cu^{2+} ions above and three below (Fig. 1 (c)). Following this recipe via the chemical synthesis of $Cu_4(OH)_6FBr$, we arrive at perfectly aligned kagome planes as shown in Fig. 1 (d). This compound is known as the mineral barlowite[15].

Single crystals of barlowite, $Cu_4(OH)_6FBr$, were grown synthetically through the hydrothermal reaction of copper carbonate basic (malachite), with perbromic acid in the presence of ammonium fluoride. The crystal structure of $Cu_4(OH)_6FBr$ was determined by single crystal X-ray diffraction measurements[17] at ambient temperature and is shown in Fig. 2. Barlowite crystallizes in $P\,6_3/mmc$ symmetry with each intralayer Cu^{2+} (Cu(1)) ion lying on a site of $2/m$ symmetry (see Table I). This intralayer Cu^{2+} exhibits a strongly tetragonally distorted octahedral coordination with four equatorial Cu-O bonds of 1.954(1) Å and two axial Cu-Br bonds of 3.022 Å. Interlayer Cu^{2+} (Cu(2)) sites lie on a general position and are thus 1/3 occupied and disordered over three equivalent positions.

In order to characterize barlowite electronically and magnetically, we combined first principles density functional theory (DFT) calculations with susceptibility measurements. Our DFT calculations were performed on the basis of the full-potential non-orthogonal local-orbital basis (FPLO)[18], employing the generalized gradient approximation (GGA)[19] as well as GGA+U[20] functionals. The Hubbard parameter U was set to 6 eV, the Hunds rule coupling J_H to 1 eV. Note that for reason of comparability with the closely related material herbertsmithite, we have here chosen the same value of U and J_H as in our previous study Ref. 21. The exchange-coupling constants between spin-1/2 Cu^{2+} ions were obtained by mapping GGA+U total energy differences of several Cu^{2+} spin configurations onto a spin-1/2 Heisenberg model[21,22]. In order to make a sufficient number of Cu^{2+} sites inequivalent to allow for various spin configurations, the symmetry was lowered from the $C\,mcm$ to the $C\,m$ space group (No. 8) containing 6 inequivalent Cu^{2+} positions.

In Fig. 3 (a)-(b) we show first the GGA band structure and density of states of barlowite. The main contribu-

TABLE I. Structural parameters for $Cu_4(OH)_6FBr$ at T = 298(2) K ($P\,6_3/mmc$ space group, a = 6.799(4) Å, c = 9.3063(13) Å, Z = 2). In this table, U is the anisotropic displacement parameter (isotropic for H).

Atom	Site	x	y	z	U (Å^2)	Occ.
Cu(1)	6g	1/2	0	0	0.01540(17)	1
Cu(2)	12j	0.62884(12)	0.2577(2)	1/4	0.0133(4)	1/3
O	12k	0.79768(18)	0.20232(18)	0.0916(2)	0.0137(4)	1
H	12k	0.852(3)	0.148(3)	0.127(4)	0.021	1
Br	2c	1/3	2/3	1/4	0.0184(2)	1
F	2b	0	0	1/4	0.0238(10)	1

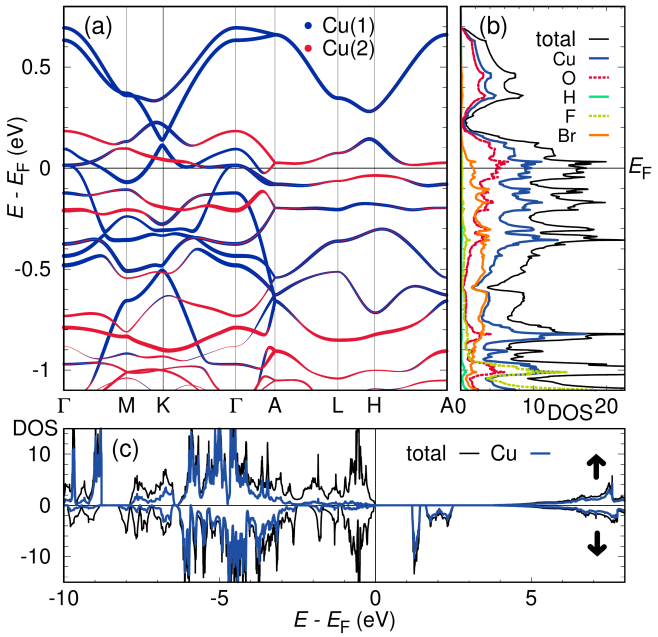

FIG. 3. (a) GGA band structure and (b) GGA density of states (DOS) of $Cu_4(OH)_6FBr$. DOS is given in states per eV and formula unit. High symmetry points $M = (1/2, 0, 0)$, $K = (1/3, 1/3, 0)$, $A = (0, 0, 1/2)$, $L = (1/2, 0, 1/2)$, $H = (1/3, 1/3, 1/2)$ were chosen to reflect the $P\,6_3/mmc$ symmetry of the real material rather than the $C\,mcm$ symmetry used for computational purposes. (c) GGA+U density of states for U = 6 eV, J_H = 1 eV and ferromagnetic order. Note that the size of the gap is related to the value of U considered.

TABLE II. Exchange coupling constants for $Cu_4(OH)_6FBr$, calculated with GGA+U at $U = 6$ eV, $J_H = 1$ eV and with atomic-limit double-counting correction. Positive (negative) J values denote antiferromagnetic (ferromagnetic) couplings.

Name	$d_{\text{Cu-Cu}}$ (Å)	Type	$J_i(K)$
	Kagome layer coupling		
J_3	3.3399	Cu(1)-Cu(1)	177
	Interlayer couplings		
J_1	2.7632	Cu(1)-Cu(2)	-205
J_2	3.1885	Cu(1)-Cu(2)	-32
J_4	4.6532	Cu(1)-Cu(1)	5
J_6	5.5264	Cu(2)-Cu(2)	16

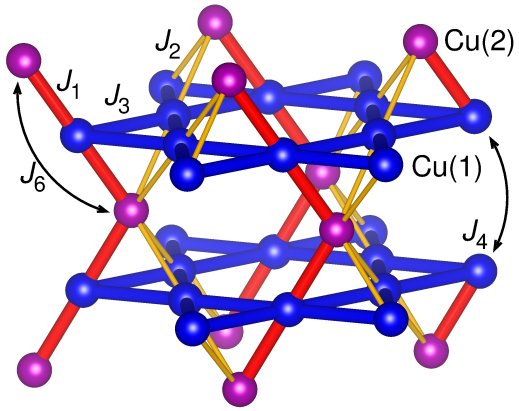

FIG. 4. Important exchange paths of $Cu_4(OH)_6FBr$ (see Table II). The notation J_i, $i = 1, 2, 3, \ldots$ denotes 1^{st}, 2^{nd}, 3^{rd},... Cu-Cu neighbors.

tion near the Fermi level is of Cu $3d$ orbitals hybridized with O $2p$ orbitals. The band structure along the high-symmetry path Γ-M-K-Γ reflects the dispersion of the kagome layers (dominated by Cu(1) d states) while the band structure along the high-symmetry path A-L-H-A at $k_z = 0.5$ arises from the 2D lattice formed by the inter-kagome Cu(2) atoms. The electronic structure of the kagome layer resembles that of the of the spin-liquid compound herbertsmithite very well[21]. However, both herbertsmithite and barlowite are Mott insulators. In order to reflect this behavior in the band structure calculations we show in Fig. 3 (c) the density of states calculated with the GGA+U functional with $U = 6$ eV.

The exchange couplings we obtain from total energy calculations are listed in Table II. The nearest neighbor coupling in the kagome plane is $J_3 = 177$ K for barlowite. This is very similar to the value $J = 182$ K obtained for herbertsmithite, reflecting the fact that Cu-O-Cu angles are very similar in both compounds (117° in barlowite, 119° in herbertsmithite). The fact that barlowite has Cu^{2+} ions at interlayer positions (Cu(2)) determines the magnetic behavior of this system at low temperatures. Specifically, we find that ferromagnetic interlayer couplings ($J_1 = -205$ K and $J_2 = -32$ K) exist between Cu(1) (in the kagome layer) and Cu(2) (interlayer). Further exchange paths become increasingly and significantly weaker – comparable or smaller than $0.1J$. Within the $C\,m$ unit cell chosen here, it was not possible to separate the coupling J_5 corresponding to a Cu(1)-Cu(2) distance of 5.2359 Å from the small ferromagnetic J_2. The vertical coupling J_4 between the kagome planes is negligibly small. The resulting Heisenberg Hamiltonian parameters are illustrated in Fig. 4. Note that due to the lowering of the symmetry from $P\,6_3/mmc$ to $C\,mcm$ for the calculations, the path of the ferromagnetic one-dimensional Cu(2) chains has become uniquely defined. In reality, these chains wiggle through the crystal according to the actual positions of Cu(2) which is randomly chosen from the three possible sites. We estimate an error bar on the Heisenberg Hamiltonian parameters of the order of 20% and possibly larger for the smaller couplings because the calculated values depend strongly on the essentially unknown size of the Hubbard parameter U and because of the tendency of DFT to overestimate the stability of the ferromagnetic state.

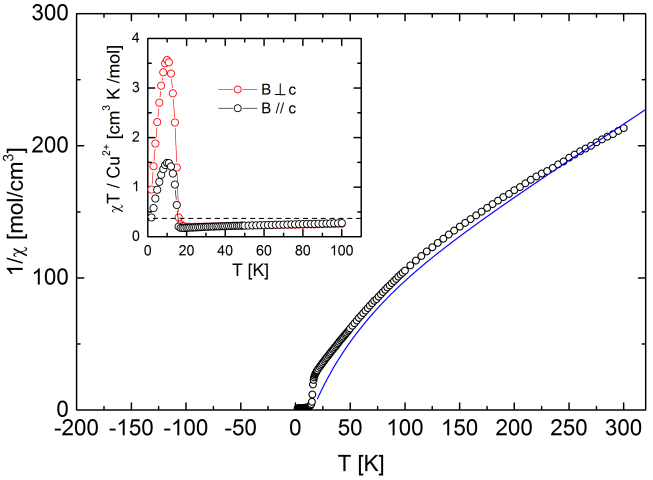

FIG. 5. Inverse molar susceptibility as a function of temperature (open circles) taken at $B = 0.1$ T for $B \parallel c$ together with a theoretical approximation to $1/\chi$ calculated by 10th-order high-temperature series expansion[23] (see main text). Inset: $\chi_{\text{mol}} \cdot T$ / Cu^{2+} ion as a function of temperature in fields $B = 0.1$ T for $B \parallel c$ and $B \perp c$ both after cooling in zero field (ZFC). The broken line indicates the value for a spin $S = 1/2$ of 0.376.

The magnetic properties of barlowite were measured using a commercial Quantum Design SQUID magnetometer in the temperature range 2 K $\leq T \leq$ 300 K on a single crystal of mass $m = 3.4$ mg. The susceptibility measurements were performed in various fields up to 1 T with orientation parallel and perpendicular to the hexagonal c-axis. For the latter orientation the magnetization was measured in fields up to ±5 T. The experimental data have been corrected for the temperature-independent diamagnetic core contribution of the constituents[26] and the magnetic contribution of the sample

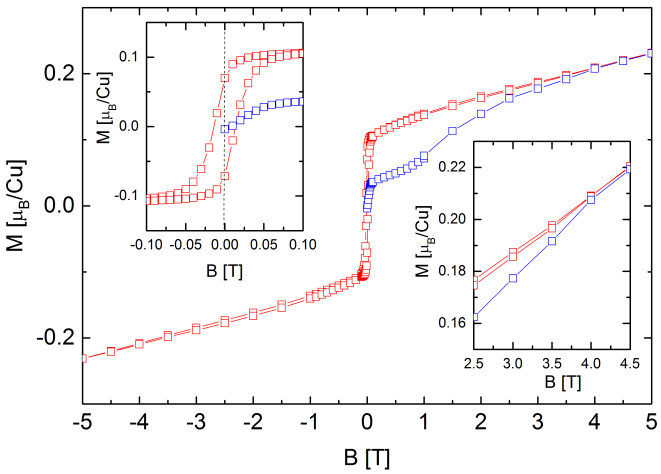

FIG. 6. Magnetization as a function of magnetic field B measured for $B \parallel c$ at $T = 2$ K. The blue open squares correspond to the virgin curve taken after cooling in zero field, the red diamonds correspond to data taken upon subsequent field cycling. Lower right inset: blow-up of high-field section. Upper left inset: blow-up of low-field section.

holder.

By considering the exchange parameters obtained from DFT, we calculated $1/\chi_{\rm mol}$ using 10th-order high-temperature series expansion[23]. The result is shown in Fig. 5 together with the experimental $1/\chi_{\rm mol}$ data for $B \parallel c$. We find that a very good fit of the experimental observations, shown by the solid line, is obtained with $J_3 = 177$ K and $J_1 = -0.94J_3$, $J_2 = -0.16J_3$ and $J_6 = 0.15J_3$ in combination with a g value of 2.20. Given the strongly distorted octahedral Cu^{2+} environment, implying anisotropic g values ranging from $0.1 \leq \Delta g/g \leq 0.15$[24,25], a g value of 2.2 for $B \parallel c$ is reasonable. The so-derived values of the exchange couplings are within the error bars of the DFT calculation confirming that the DFT analysis of barlowite is reliable.

The inset of Fig. 5 exhibits $\chi_{\rm mol} \cdot T$ / Cu^{2+} ion as a function of temperature for $T \leq 100$ K in fields $B = 0.1$ T for $B \parallel c$ and $B \perp c$ both after cooling in zero field (ZFC). At 300 K (not shown) $\chi_{\rm mol} \cdot T$ is about 0.367, a value slightly smaller than the one for isolated spin-1/2 ions. With decreasing temperature $\chi_{\rm mol} \cdot T$ becomes continuously reduced down to approximately 0.261 around 20 K. Such a large $\chi_{\rm mol} \cdot T$ value in an antiferromagnetically coupled system at a temperature $T \lesssim J_3/10$ is only possible when in addition a ferromagnetic coupling exists which is of similar size. Upon cooling to below about 18 K, $\chi_{\rm mol} \cdot T$ for both orientations starts to increase with a maximum slope around 15 K, followed by a pronounced maximum. The overall magnetic response, especially the steep increase of $\chi_{\rm mol} \cdot T$ in the paramagnetic phase close to T_N, is a clear signature of a phase transition into long-range antiferromagnetic order characterized by canted spins exhibiting a small ferromagnetic component[27]. The maximum of $\chi_{\rm mol} \cdot T$ for $B \perp c$ exceeds that for $B \parallel c$ by more than a factor of two. These temperature- and orientation-dependences indicate that the easy axes are tilted against the kagome plane.

Figure 6 exhibits the magnetization measured for $B \parallel c$ at 2 K. The blue open squares correspond to the virgin curve taken after cooling in zero field. This was possible after carefully compensating for finite remanent fields present in the superconducting magnet of the SQUID magnetometer. Also shown is the full hysteresis loop obtained upon cycling the field in the range -5 T $\leq B \leq +5$ T. The hysteresis loop closes at $|B| \geq 4$ T at 2 K, cf. lower right inset to Fig. 6. Upon field cycling (red symbols), following the virgin run, the magnetization exhibits a large slope for fields below 0.1 T. At this field level, M reaches approximately 10% of the expected saturation magnetization of 1 $\mu_{\rm B}$ per Cu^{2+} ion. On further increasing the field $M(B)$ increases almost linearly and reaches a value of 0.23 $\mu_{\rm B}/Cu^{2+}$ at 5 T, which is close to 1 $\mu_{\rm B}$/f.u. The upper inset of Fig. 6 shows the low-field sector of the hysteresis loop. For $B = 0$ barlowite has a remanent magnetization of approximately 0.075 $\mu_{\rm B}$/Cu. According to Ref. 26 this value together with the saturation magnetization can be used to determine the tilt angle relative to the perfectly antiferromagnetically aligned spins resulting in a canting angle of approximately 4.5°. We assign the difference between this canting angle and the orientation of the basal plane of the Cu octahedra to the existence of a Dzyaloshinskii-Moriya (DM) interaction allowed by symmetry in barlowite which acts here like an easy-plane anisotropy. The DM vector $\mathbf{D}$ lies within the mirror plane [27] which in barlowite is perpendicular to the kagome plane. An estimate of the size of $|\mathbf{D}|$ is given by $|\mathbf{D}|/J_3 \simeq \Delta g/g = 0.1$ which is substantial. As worked out in detail in Ref. [28] the DM-interaction in frustrated kagome systems can induce a long range canted antiferromagnetic order. According to Ref. [28] we can conclude from our experimental findings that $\mathbf{D}$ is definitely not perpendicular to the kagome plane. In contrast, it has a significant in-plane component D_p.

According to our calculations, cf. Table II, there are no ferromagnetic interactions between the interlayer Cu(2) ions larger than $0.1J_1$, which rules out that the weak ferromagnetism originates from ordering among these interlayer spins. However, the interlayer spins influence the magnetization in the ordered state. There are strong (J_1) and moderate (J_2) ferromagnetic couplings between the spins in the kagome plane (Cu(1)) and the interlayer spins (Cu(2)). As a result there are no degrees of freedom left for the Cu(2) spins in fields which are small compared to these couplings. The spins align parallel to the Cu(1) spins belonging to the kagome layers and are thus also tilted against the kagome planes. They contribute to the remanent magnetization according to their relative abundance (25%).

In summary, as exemplarily shown for barlowite, we propose a new synthetic route for kagome-based structures with the possibility of interesting phases such as

ordered magnetic phases with different ordering vectors, spin liquid, Dirac metal or even unconventional superconductivity. On the one hand, substitutions at the interlayer cation site[14] may be effective for the realization of such states; on the other hand, the existence of the mineral claringbullite $Cu_4(OH)_6FCl$[29,30] which is isostructural to barlowite but has different combinations of anions – the Br^- ion of barlowite is replaced by Cl^- – demonstrates that the synthesis route outlined here opens the path to a family of compounds. Finally, our combined first principles calculations with susceptibility measurements identifies the low temperature behavior of barlowite as a canted antiferromagnet with a canting angle of approximately 4.5°.

Acknowledgements.- We would like to thank the Deutsche Forschungsgemeinschaft for financial support through the collaborative research unit TRR/SFB 49. F.S.-P. gratefully acknowledges the support of the Alexander von Humboldt Foundation through a Humboldt Research Fellowship. J.A.S. acknowledges support from the Independent Research/Development program while serving at the National Science Foundation.

[1] M. P. Shores, E. A. Nytko, B. M. Bartlett and D. G. Nocera, A structurally perfect $S = 1/2$ kagomé antiferromagnet, J. Am. Chem. Soc. **127**, 13462 (2005).

[2] P. Mendels and F. Bert, Quantum kagome antiferromagnet $ZnCu_3(OH)_6Cl_2$, J. Phys. Soc. Jpn. **79**, 011001 (2010).

[3] P. Mendels and F. Bert, Quantum kagome antiferromagnet: $ZnCu_3(OH)_6Cl_2$, J. Phys.: Conf. Series **320**, 012004 (2011).

[4] S.-H. Lee, H. Kikuchi, Y. Qiu, B. Lake, Q. Huang, K. Habicht, and K. Kiefer, Quantum-spin-liquid states in the two-dimensional kagome antiferromagnets $Zn_xCu_{4x}(OD)_6Cl_2$, Nat. Mater. **6**, 853 (2007).

[5] R. H. Colman, A. Sinclair, and A. S. Wills, Magnetic and crystallographic studies of Mg-herbertsmithite, γ-$Cu_3Mg(OH)_6Cl_2$ – A new $S = 1/2$ kagome magnet and candidate spin liquid, Chem. Mater. **23**, 1811 (2011).

[6] Y. Li, B. Pan, S. Li, W. Tong, L. Ling, Z. Yang, J. Wang, Z. Cheng, Z. Wu and Q. Zhang, Gapless quantum spin liquid in the $S = 1/2$ anisotropic kagome antiferromagnet $ZnCu_3(OH)_6SO_4$, New J. Phys. **16**, 093011 (2014).

[7] Y.-S. Li, Q.-M. Zhang, Structure and magnetism of $S = 1/2$ kagome antiferromagnets $NiCu_3(OH)_6Cl_2$ and $CoCu_3(OH)_6Cl_2$, J. Phys. Condens. Matter **25**, 026003 (2013).

[8] P. A. Lee, An end to the drought of quantum spin liquids, Science **321**, 1306 (2008).

[9] Y. Shimizu, K. Miyagawa, K. Kanoda, M. Maesato, G. Saito, Phys. Rev. Lett. **91**, 107001 (2003).

[10] T. Itou, A. Oyamada, S. Maegawa, M. Tamura, R. Kato, Spin liquid state in an organic Mott insulator with a triangular lattice, Phys. Rev. B **77**, 104413 (2008).

[11] T.-H. Han, J. S. Helton, S. Chu, D. G. Nocera, J. A. Rodriguez-Rivera, C. Broholm, Y. S. Lee, Fractionalized excitations in the spin-liquid state of a kagome-lattice antiferromagnet, Nature **492**, 406 (2012).

[12] D. E. Freedman, T. H. Han, A. Prodi, Peter Müller, Q.-Z. Huang, Y.-S. Chen, S. M. Webb, Y. S. Lee, T. M. McQueen, and D. G. Nocera, Site specific x-ray anomalous dispersion of the geometrically frustrated kagomé magnet, herbertsmithite, $ZnCu_3(OH)_6Cl_2$, J. Am. Chem. Soc. **132**, 16185 (2010).

[13] T. Hanisch, G. S. Uhrig, and E. Müller-Hartmann, Lattice dependence of saturated ferromagnetism in the Hubbard model, Phys. Rev. B **56**, 13960 (1997).

[14] I. I. Mazin, H. O. Jeschke, F. Lechermann, H. Lee, M. Fink, R. Thomale, and R. Valentí, Theoretical prediction of a strongly correlated Dirac metal, Nat. Commun. **5**, 4261 (2014).

[15] P. Elliott, and M. A. Cooper, New minerals and nomenclature modifications approved in 2010, Mineralog. Mag. **74**, 797 (2010).

[16] T.-H. Han, J. Singleton, and J. Schlueter, Barlowite: A spin-1/2 antiferromagnet with a geometrically perfect kagome motif, Phys. Rev. Lett. **113**, 227203 (2014).

[17] CCDC 1019246 contains the supplementary crystallographic data for this paper. These data can be obtained free of charge from The Cambridge Crystallographic Data Centre via `www.ccdc.cam.ac.uk/data_request/cif`.

[18] K. Koepernik and H. Eschrig, Full-potential nonorthogonal local-orbital minimum-basis band-structure scheme, Phys. Rev. B **59**, 1743 (1999); http://www.FPLO.de

[19] J. P. Perdew, K. Burke, and M. Ernzerhof, Generalized gradient approximation made simple, Phys. Rev. Lett. **77**, 3865 (1996).

[20] A. I. Liechtenstein, V. I. Anisimov, and J. Zaanen, Density functional theory and strong interactions: Orbital ordering in Mott-Hubbard insulators, Phys. Rev. B **52**, R5467 (1995).

[21] H. O. Jeschke, F. Salvat-Pujol, R. Valentí, First-principles determination of Heisenberg Hamiltonian parameters for the spin-1/2 kagome antiferromagnet $ZnCu_3(OH)_6Cl_2$, Phys. Rev. B **88**, 075106 (2013).

[22] K. Foyevtsova, I. Opahle, Y.-Z. Zhang, H. O. Jeschke, R. Valentí, Determination of effective microscopic models for the frustrated antiferromagnets Cs_2CuCl_4 and Cs_2CuBr_4 by density functional methods, Phys. Rev. B **83**, 125126 (2011).

[23] A. Lohmann, H.-J. Schmidt, J. Richter, Tenth-order high-temperature expansion for the susceptibility and the specific heat of spin-s Heisenberg models with arbitrary exchange patterns: Application to pyrochlore and kagome magnets, Phys. Rev. B **89**, 014415 (2014).

[24] B. L. Silver and D. Getz, ESR of $Cu^{2+}(H_2O)_6$. II. A quantitative study of the dynamic Jahn-Teller effect in copper-doped zinc Tutton's salt, J. Chem. Phys. **61**, 638 (1973).

[25] V. E. Petrashen, Yu. V. Yablokov, and R. L. Davidovich, The lattice structure parameters and configuration of Cu^{2+} Jahn-Teller centres in Tutton salt crystals, Phys. Stat. Sol. B **101**, 117 (1980).

[26] O. Kahn, *Molecular Magnetism*, VCH, Weinheim-New York, 1993.

[27] T. Moriya, Anisotropic superexchange interaction and weak ferromagnetism, Phys. Rev. **120**, 91 (1960).

[28] M. Elhajal, B. Canals, C. Lacroix, Symmetry breaking due

to Dzyaloshinsky-Moriya interactions in the kagomé lattice, Phys. Rev. B **66**, 014422 (2002).

[29] E. E. Fejer, A. M. Clark, A. G. Couper, and C. J. Elliott, Claringbullite, a new hydrated copper chloride, Mineralog. Mag. **41**, 433 (1977).

[30] M. S. Rumsey, M. D. Welch, M. J. Origlieri, G. Cressey, A. R. Kampf, L. Burgio, J. Spratt, and E. R. Humphreys-Williams, E. R., A redefinition of claringbullite to $Cu_4ClF(OH)_6$; the importance of type material and group/series based studies, 21st General Meeting of the International Mineralogical Association, Abstract Volume, p. 375 (2014).